RESEARCH ARTICLE

Sustainable Energy

Energy & Environmental Materials WILEY

Closing the Loop in Agrivoltaics: A Radiative Cooling Coating for Synergistic Self-Cleaning and Water Harvesting

*Saichao Dang, Abdul Rahim Siddiqui, Murali Gedda, Yuxuan Huang, Shakeel Ahmad, Jehad K. El-Demellawi, Dan Daniel, Osman M. Bakr, Stefaan De Wolf, Hussam Qasem, Husam N. Alshareef, and Qiaoqiang Gan**

The integration of photovoltaic (PV) panels into agricultural landscapes (i.e., agrivoltaics) offers a promising path for sustainable land use, yet its potential is limited by dust soiling and water scarcity. Current cleaning methods are often water-intensive, costly, or ecologically detrimental. Here, we introduce a multifunctional coating that synergistically couples PV panels with the microclimate to address these intertwined challenges. Fabricated via a simple, solvent-free process from a food-grade silicone, the coating is highly transparent (∼91.3%, 350–1100 nm) and superhydrophobic (contact angle: 167°, sliding angle: 3°). Crucially, its high emissivity (0.90) in the atmospheric window (8–13 µm) enhances radiative cooling, passively inducing nighttime condensation. This condensation triggers a self-cleaning mechanism, where shedding droplets autonomously remove dust, and simultaneously enables atmospheric water harvesting. In 6-month outdoor tests in Saudi Arabia, coated panels maintained performance with only ∼1.5% power loss, compared to ∼28% for uncoated panels. Furthermore, the system achieved a dew yield of 128 g m^{-2} per night—over twice that of untreated surfaces—providing a water source sufficient for irrigating co-located crops (demonstrated with *Brassica rapa chinensis*). This work transformed the PV panel from a passive energy harvester into an active hub that ensures its own performance while supporting on-site agriculture, establishing a resilient and self-sustaining nexus for energy, water, and food security.

1. Introduction

The global expansion of photovoltaic (PV) deployment has established solar energy as a cornerstone of the clean energy transition.[1,2] This rapid growth necessitates system-level innovations that maximize land-use efficiency and operational resilience. Agrivoltaics—the co-location of solar energy generation and agricultural production—has emerged as a promising strategy to reinforce the food–energy–water nexus.[3,4] These systems are particularly valuable in sun-rich, arid regions, such as the Middle East and North Africa, which possess abundant solar resources but face chronic challenges of food and water scarcity.[2,3]

In these regions, a critical barrier to implementing this vision is dust accumulation, which severely compromises the long-term performance and economic viability of PV systems.[5–7] Deposited particulates obstruct sunlight and elevate module temperatures, leading to efficiency losses of 20–50% within weeks.[7,8] Even a minimal dust layer (∼5 g m^{-2}) can reduce power output by 10–15%, and interactions with dew can form hardened crusts that resist removal.[9] Furthermore, dust acts as a thermal insulator; given that silicon PV cells lose ∼0.3–0.5% efficiency per °C temperature rise,[10–12] the combined optical and thermal effects significantly accelerate performance degradation. These issues are compounded by bio-soiling like bird droppings, where a single spot covering 5% of a panel can reduce output by over 30%.[13,14] Consequently, developing autonomous, low-maintenance cleaning solutions is imperative to sustain solar productivity.

To overcome this barrier and unlock the full potential of synergistic agrivoltaics, a PV surface must be engineered to simultaneously fulfill multiple, often conflicting, functional requirements: 1) high optical transmittance across the solar spectrum (350–1100 nm) to maximize energy generation;[15,16] 2) strong mid-infrared thermal emissivity to enhance radiative cooling (RC) and promote nighttime condensation;[17–19] 3) nanoscale texturing to provide abundant nucleation sites for efficient droplet formation;[20–22] and 4) superhydrophobic or slippery characteristics to ensure rapid droplet shedding for autonomous cleaning and irrigation.[6,15] While these individual properties have been demonstrated in isolation,[23–26] their integration into

Dr. S. Dang, Dr. A. R. Siddiqui, Dr. M. Gedda, Dr. Y. Huang, Dr. S. Ahmad, Q. Gan
Sustainable Photonics Energy Research Laboratory, Materials Science and Engineering, Physical Sciences and Engineering Division (PSE), King Abdullah University of Science and Technology (KAUST), Thuwal 23955-6900, Saudi Arabia
E-mail: qiaoqiang.gan@kaust.edu.sa
Dr. J. K. El-Demellawi, Prof. S. De Wolf, H. N. Alshareef, Q. Gan
Center for Renewable Energy and Storage Technologies (CREST), KAUST, Thuwal 23955-6900, Saudi Arabia
Prof. D. Daniel
Droplet Lab, Mechanical Engineering, PSE, KAUST, Thuwal 23955-6900, Saudi Arabia
Prof. O. M. Bakr
Functional Nanomaterials Laboratory, Materials Science and Engineering, PSE, KAUST, Thuwal 23955-6900, Saudi Arabia
Prof. S. De Wolf, H. N. Alshareef
KAUST Solar Platform, PSE, KAUST, Thuwal 23955-6900, Saudi Arabia
Prof. H. Qasem
Future Energy Technology Institute, King Abdulaziz City for Science and Technology, Riyadh 11442, Saudi Arabia
The ORCID identification number(s) for the author(s) of this article can be found under https://doi.org/10.1002/eem2.70350.

DOI: 10.1002/eem2.70350

© 2026 The Author(s). *Energy & Environmental Materials* published by John Wiley & Sons Australia, Ltd on behalf of Zhengzhou University. This is an open access article under the terms of the Creative Commons Attribution License, which permits use, distribution and reproduction in any medium, provided the original work is properly cited.

a single, scalable, and durable coating has remained an unmet scientific and technological challenge, preventing the realization of a truly self-sustaining agrivoltaics system.

Here, we bridge this gap by introducing a rationally designed photonic–thermal coating that integrates these functionalities through nanoscale structural engineering. Fabricated through a simple, solvent-free thermal treatment of a food-grade silicone lubricant, our coating achieves high solar transmittance (∼91.3%), high mid-infrared emissivity (∼0.9), and superhydrophobicity (contact angle ∼167°). This combination enables a self-sustaining operational loop: the coating's high emissivity drives radiative cooling and enhances nighttime dew formation, while its superhydrophobic nanostructure promotes droplet coalescence and rapid shedding for passive dust removal. During 6 months of outdoor testing in Saudi Arabia, coated PV modules maintained performance with only a 0.29% efficiency loss, compared to 3.21% for uncoated modules—a net relative gain of approximately 3%. Beyond self-cleaning, this RC-driven process also enabled efficient atmospheric water harvesting, yielding 128 g m^{-2} per night, which we successfully used to irrigate *Brassica rapa chinensis*. This work establishes a transformative material strategy that moves beyond passive functionality, enabling PV panels to become active participants in a resilient and self-sustaining ecosystem for energy, water, and food security.

2. Results and Discussion

2.1. Optimized Agrivoltaics and Challenges: The Synergistic PV–Water–Agriculture Loop

The essential elements of an agrivoltaics system are shown in **Figure 1a**. Photovoltaic (PV) panels provide shading that mitigates crop heat stress and suppresses soil water loss, while crops release moisture through transpiration, increasing local humidity and contributing to passive cooling of the panels (left panel in Figure 1a).[3] When coupled with enhanced nighttime radiative cooling (RC), this interaction can be extended into a fully integrated operational loop: RC drives surface condensation on the PV module, the resulting droplets remove deposited dust, and the harvested water can be redirected to support plant irrigation (right panel in Figure 1a). This closed-loop synergy couples energy production, water generation, and agricultural productivity within a unified land-use framework (Figure 1b).

Realizing such a loop requires a PV surface that satisfies four demanding functional criteria simultaneously: high solar transmittance, strong mid-infrared (MIR) emissivity, abundant nanoscale nucleation sites for dew formation, and rapid droplet shedding for autonomous cleaning. Achieving all four properties in a single material is nontrivial. Conventional engineering approaches typically optimize one or two—such as visible-light management or hydrophobicity—but compromise the others because the underlying optical, thermal, and wetting mechanisms are often antagonistic.[6] For example, subwavelength "moth-eye" nanostructures are effective at minimizing reflection and boosting visible-light transmittance,[27,28] yet it remains unclear whether such patterns can also promote efficient condensation nucleation[20,21] or support the high MIR emissivity required for strong RC.[18,25,26,29–30] Similarly, superhydrophobic or slippery surfaces generally rely on hierarchical textures or infused lubricants that can degrade optical clarity[31,32] or alter thermal-radiative properties.[33,34] These competing constraints have prevented the development of a coating capable of unifying optical transparency, RC enhancement, and autonomous droplet management.

2.2. Simultaneous Visible and Mid-Infrared Optical Coating

Here we introduce a photonic–thermal coating that resolves these long-standing conflicts by integrating nanoscale texturing with a solvent-free, thermally reorganized silicone layer. This rational design simultaneously delivers high solar transmittance, strong MIR emissivity, and robust superhydrophobicity—meeting all four functional criteria without trade-offs. As discussed below, this multifunctional surface enables PV modules not only to resist soiling but also to become active agents in water harvesting and agricultural support, thereby operationalizing the self-sustaining agrivoltaics cycle.

Figure 2a shows the coating procedure by casting a food-grade silicone-based lubricant onto transparent glass, followed by a single-step thermal annealing process at 400 °C for 30 min (details in Note S1, Supporting Information). These food-grade silicone lubricants are composite systems consisting of a polydimethylsiloxane (PDMS) fluid and fumed-silica nanoparticle fillers that act as thickeners. Upon heating, the volatile silicone oil phase and minor additives decompose, yielding a nanostructured surface texture, as confirmed by scanning electron microscopy (SEM, Figure 2b). For practical deployment, the coating should maintain uniformity and transparency over large areas, which was demonstrated by its successful application to a 20 × 20 cm^2 glass panel (Figure 2c), confirming scalability and compatibility with photovoltaic modules. This hierarchical structure is produced via a simple, scalable one-step process, avoiding complex top-down fabrication techniques.[33]

The detailed surface morphology was characterized by atomic force microscopy (AFM), as shown in Figure 2d. The initially smooth glass substrate (RMS roughness ∼1.4 nm) is transformed into a hierarchically textured surface featuring nanoscale peaks and valleys with heights below 180 nm and RMS roughness of ∼82 nm, which are subwavelength relative to the operational range of silicon photovoltaic cells (350–-1100 nm).[27,28] A comparative AFM analysis of the coated and uncoated surfaces is provided in Note S2, Supporting Information. The formation of this hierarchical topography is attributed to a filler-templated pyrolytic structuring

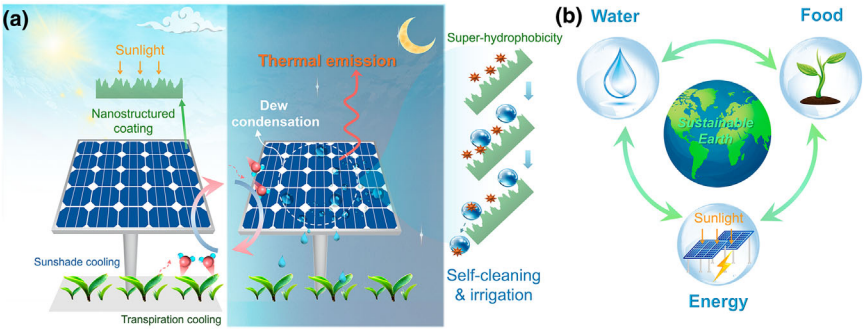


Figure 1. Concept illustration of the synergistic PV–water–agriculture loop by using RC-induced water condensation for autonomous PV cleaning and crop irrigation (a) for water–food–energy nexus (b).

© 2026 The Author(s). *Energy & Environmental Materials* published by John Wiley & Sons Australia, Ltd on behalf of Zhengzhou University.

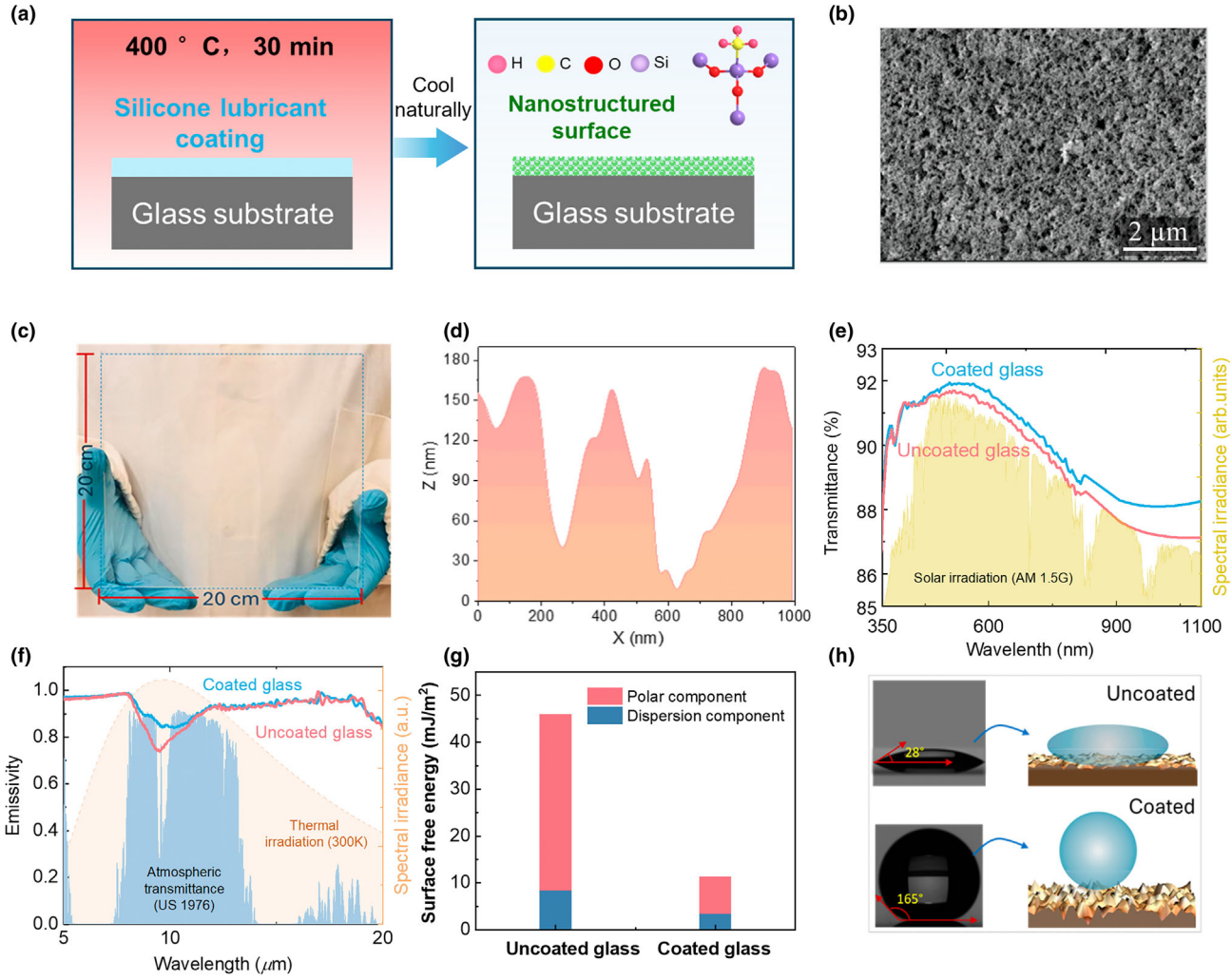


Figure 2. Fabrication, characterization of the performance of the transparent superhydrophobic coating. a) Schematic illustration of the fabrication process: a food-grade silicone-based lubricant is cast onto glass and thermally annealed in a single step to generate a nanostructured surface. b) Scanning electron microscopy (SEM) image showing the nanostructured morphology of the coated surface. c) Photograph demonstrating the high visual transparency of the coated glass (20×20 cm^2). d) Atomic force microscopy profile revealing hierarchical surface topography with subwavelength peaks and valleys within a scale of height $<$180 nm. e) Measured transmittance spectra of coated and uncoated glass substrates in the 380–1300 nm range, showing slightly enhanced transmission after coating. f) Mid-infrared emissivity spectra of coated and uncoated samples, indicating enhanced emissivity in the atmospheric window (8–13 μm). g) Surface free energy analysis (dispersive and polar components) derived from contact angle measurements, confirming reduced surface energy upon coating. h) Static water contact angle measurements showing hydrophilic behavior of uncoated glass (∼28°) and superhydrophobicity (∼165°) after coating.

mechanism. During annealing, the PDMS matrix undergoes thermo-oxidative shrinkage, whereas the fumed silica nanoparticles remain rigid and non-shrinking. This mechanical mismatch induces surface stresses that kinetically imprint the filler network into the coating, resulting in the observed nanoscale roughness. Such hierarchical structuring is essential for achieving enhanced solar-band transmittance, increased mid-infrared emission, and robust superhydrophobicity. In particular, the nanoscale peaks and valleys provide abundant nucleation sites, promoting efficient condensation.

As shown in Figure 2e, the coated glass exhibits a high transmittance of 91.3% across the working wavelength range of silicon photovoltaic cells (350–1100 nm),[15,16] which is 1.4% higher than that of the uncoated glass. This improvement arises from surface-scattering–induced anti-reflection effects on the hierarchical rough surface, similar to the moth-eye structure, potentially enhancing photovoltaic performance.[35] In the mid-infrared (MIR) region, the hierarchical surface roughness of the coating also leads to a slight enhancement in emissivity, particularly within the atmospheric transparency window (8–13 μm),[18] as evidenced by the higher spectral emissivity of the coated glass compared to the uncoated counterpart in Figure 2f. This emissivity enhancement indicates a modest improvement in the radiative cooling capability relative to the uncoated glass, which will be discussed in detail in the later section.

2.3. Superhydrophobicity

Upon heating, the volatile silicone oil phase along with minor additives decomposes, forming a silica-based framework primarily composed of a

© 2026 The Author(s). *Energy & Environmental Materials* published by John Wiley & Sons Australia, Ltd on behalf of Zhengzhou University.

Si–O–Si network, while some surface-bound hydrophobic Si–CH_3 groups are retained (inset in Figure 2b).[36–38] At higher annealing temperatures (e.g., 500 °C), however, these low-surface-energy methyl groups are further oxidized and removed, exposing polar Si–OH groups and resulting in a transition to hydrophilic surface behavior (for a detailed discussion of temperature-dependent surface chemistry, wettability, and underlying mechanisms, see Note S3, Supporting Information).[39] Surface free energy analysis, including dispersive and polar components (Figure 2g), further confirms the substantially reduced surface energy of the coated glass, supporting its superhydrophobic behavior. The resulting nanoscale surface roughness also enhances air trapping beneath water droplets and minimizes solid–liquid contact area, which are critical for achieving superhydrophobicity.[20,21] As illustrated in Figure 2h, uncoated glass exhibits hydrophilic behavior with a water contact angle of 28°, whereas the coated surface shows superhydrophobicity with a contact angle of 165°, reflecting the combined effects of low surface energy and hierarchical surface architecture.

2.4. RC-Induced Dew Condensation Analysis

The radiative cooling (RC) performance that drives nighttime dew condensation is fundamentally governed by the net energy exchange between the emitter and its surroundings. For a PV panel coating in an outdoor nighttime environment, the energy balance can be described as:[18]

$$P_{net} = P_{rad}(\varepsilon(\lambda), T) - P_{atm}(t(\lambda), T_{atm}) - P_{non-rad}(h_{non}) \quad (1)$$

here, P_{rad} is the outgoing thermal radiation power from the panel surface; P_{atm} is the downward atmospheric thermal radiation absorbed by the panel; $P_{non\text{-}rad}$ is the power gain caused by non-radiative heat exchange. The net cooling power can be quantitatively evaluated by incorporating the spectral emissivity $\varepsilon(\lambda)$, the atmospheric transparent window $t(\lambda)$ (e.g., the blue-shaded area in Figure 2f), and the non-radiative heat transfer coefficient h_{non} (see Note S4, Supporting Information, for detailed calculations). In particular, the slight increase in emissivity from 0.87 to 0.90 introduced by the nanostructured coating enhances the net cooling power by 13 W m^{-2}, thereby creating more favorable thermodynamic conditions for dew condensation on the coated surface (see Note S4, Supporting Information, for detailed calculations).

To evaluate the temperature reduction performance of the coated glass, we calculated the equilibrium temperature by incorporating ambient temperature and relative humidity (RH), as shown in **Figure 3a**. It should be noted that water vapor absorbs thermal radiation in the MIR region; therefore, as RH increases, atmospheric transmittance decreases,[40] which in turn raises P_{atm} and lowers the maximum achievable subambient cooling potential.[29] For instance, at an ambient temperature of 20 °C, the predicted temperature reduction due to RC reaches 8.0 °C at 50% RH but decreases to 6.1 °C at 90% RH. To assess whether RC can induce condensation, we also calculated the dew point temperature (T_{dew_point}), which depends on ambient temperature and RH:[18]

$$T_{dew_point} = \frac{243.12\left[\ln(RH) + \frac{17.62\times T_{amb}}{243.12\times T_{amb}}\right]}{17.62 - \left[\ln(RH) + \frac{17.62\times T_{amb}}{243.12\times T_{amb}}\right]} \quad (2)$$

Condensation occurs when the surface temperature falls below T_{dew_point}, a threshold that becomes easier to reach at higher RH values. As shown in Figure 3b, at $T_{amb} = 20$ °C, the temperature drop required to reach the dew point is 10.9 °C at 50% RH, but only 1.9 °C at 90% RH—highlighting the critical role of RH in enabling condensation under various atmospheric conditions. By combining the predicted RC performance (Figure 3a) and dew point thresholds (Figure 3b), we identify the operational regimes for condensation ($T_{panel} < T_{dew_point}$), highlighted as colored zones in Figure 3c. For example, at $T_{amb} = 20$ °C, condensation on the coated glass occurs only when RH exceeds 65%.

This analysis indicates that RC-induced condensation becomes particularly effective under sufficiently humid environmental conditions. In an agrivoltaics system, transpiration from crops increases the local humidity around PV panels, further promoting nighttime condensation. When such condensate forms on a superhydrophobic surface, the droplets readily roll off due to low adhesion, removing dust particles and enabling passive self-cleaning of the PV modules (Figure 1a). In addition, the runoff droplets can be collected for supplemental agricultural irrigation, thereby closing the synergistic PV–water–agriculture loop.

2.5. Dew Self-Cleaning Demonstration

To verify the condensation-induced self-cleaning capability of the coating, we performed experiments in a controlled environmental chamber, as illustrated in Figure 3d. A cooling plate, connected to a recirculating chiller, was used to reduce the surface temperatures of both coated and uncoated glass samples to over 10 °C below ambient conditions. Simultaneously, a humidifier was used to raise the relative humidity of the chamber to approximately 90%, thereby accelerating condensation (see Note S5, Supporting Information, for further details). Under these conditions, water droplets formed on both surfaces via atmospheric moisture condensation, as recorded in Video S1, Supporting Information, and shown in Figure 3e, which provides a side-by-side visual comparison of the two surfaces during the condensation process. On the coated glass, the nanoscale surface features served as abundant nucleation sites, promoting the initial condensation of water droplets.[20,21] The droplets subsequently grew and spontaneously rolled off under gravity, efficiently removing particulate contaminants due to the high water contact angle—key features of superhydrophobicity. In contrast, condensation on the uncoated glass was sparse, and dust or methyl orange particles remained adhered even after droplet formation and runoff, leaving visible residues. These findings confirm that our transparent coating successfully integrates superhydrophobicity with condensation-based cleaning, enabling a fully passive, water- and energy-free self-cleaning mechanism. By integrating PV-panel self-cleaning with water collection for irrigation, the coating demonstrates the potential to establish a synergistic PV–water–agriculture loop, fostering a resilient, self-sustaining system that simultaneously enhances energy capture and agricultural productivity. The practical implementation and field applicability of this integrated loop will be examined in the later section.

2.6. Dust Resist Performance and Long-Term Durability

While the previous section highlighted the potential for radiative cooling–induced dew condensation and droplet-mediated self-cleaning, the resistance of the coating to various contaminants and its long-term durability should be further evaluated to address practical outdoor

© 2026 The Author(s). *Energy & Environmental Materials* published by John Wiley & Sons Australia, Ltd on behalf of Zhengzhou University.

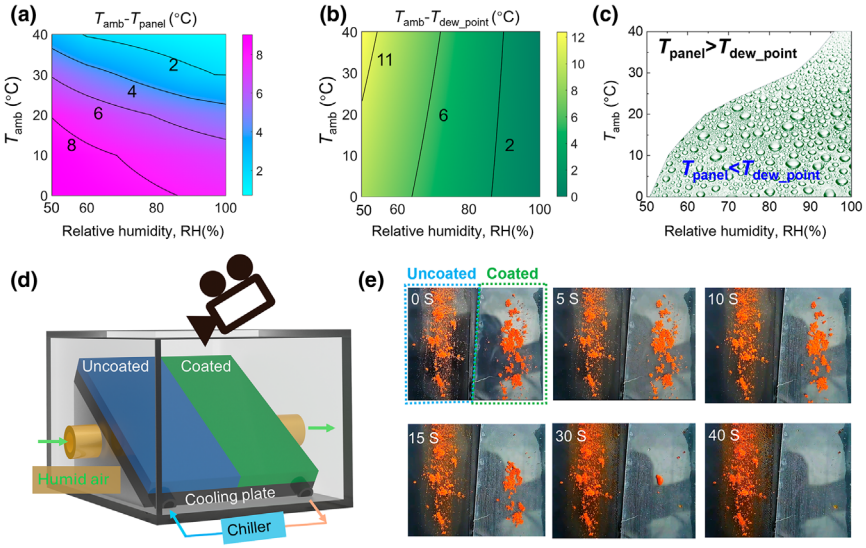


Figure 3. RC-Induced Dew Condensation Analysis and Self-Cleaning Performance. a) Simulated subambient temperature reduction ($T_{amb} - T_{panel}$) for the coated glass as a function of ambient temperature and relative humidity. b) Corresponding dew point depression ($T_{amb} - T_{dew_point}$) under various RH and temperature conditions, defining the thermodynamic window for condensation. c) Condensation is enabled when the panel temperature falls below the dew point, demonstrating the feasibility of water harvesting and moisture-driven self-cleaning. d) Schematic of the experimental setup for condensation-driven self-cleaning inside a humidity-controlled chamber. Coated and uncoated glass samples are placed on a cooling plate connected to a recirculating chiller to induce condensation. e) Time-sequenced images comparing the self-cleaning behavior of coated and uncoated samples contaminated with methyl orange particles. On the coated surface, condensed water droplets roll off spontaneously, entraining particulates and restoring surface cleanliness. In contrast, the uncoated surface retains visible contamination.

challenges, particularly those associated with dust accumulation, which can significantly degrade solar cell performance (see Note S6, Supporting Information, for quantitative data). The self-cleaning capability of the proposed coating arises from its superhydrophobic surface, which enables contaminant removal via gravitational and aerodynamic forces. To assess its practical effectiveness, the coated glass was exposed to a range of representative soiling agents—sticky bird droppings, slurry, muddy water, and cement particles—chosen to replicate common outdoor fouling scenarios (see Note S7 and Video S2–S6, Supporting Information, for more details and soiling agents). As shown in **Figure 4a**, bird droppings adhered strongly to the uncoated glass, completely obscuring the underlying KAUST logo. In contrast, on the coated surface, they formed discrete droplets that rolled off readily, leaving no visible residue (see Note S7 and Video S2, Supporting Information). Dried bird droppings are notoriously difficult to remove, highlighting the coating's real-world maintenance advantage. A similar trend was observed for slurry contamination (Figure 4b, Video S3, Supporting Information). For low-viscosity contaminants such as muddy water, the uncoated surface became heavily soiled, whereas the coated surface shed droplets cleanly without residual staining (Figure 4b, Video S4, Supporting Information). Particulate contaminants such as cements or dusts, which typically cling to conventional glass, detached easily from the coated surface with minimal disturbance, restoring transparency without mechanical cleaning (Videos S5 and S6, Supporting Information). In addition, the superhydrophobic surface enhances wind-driven dust removal.[33] As shown in Figure 4c, under identical wind exposure, dust was efficiently blown off the coated glass while remaining largely adhered to the uncoated counterpart (see details in Note S8 and Videos S7, Supporting Information). Overall, these results demonstrate that the transparent superhydrophobic coating delivers multi-modal self-cleaning performance, making it highly effective for preserving light transmission and surface cleanliness in solar panel applications.

For practical implementation, it is essential that the coating exhibits robust long-term durability under harsh outdoor conditions. In real-world applications, PV module coatings are exposed to multiple stressors, including intense solar radiation, high humidity, airborne contaminants, and thermal loads from nearby electronic components. An effective anti-soiling solution must sustain stable optical and wetting performance under such conditions without frequent maintenance. However, many previously reported superhydrophobic coatings[6,15,41] and commercial offerings[8,32] have not undergone systematic long-term durability evaluations, leaving their reliability in real-world settings uncertain. To address this critical gap, we conducted a series of accelerated aging and environmental exposure tests to assess the performance stability of the proposed coating under conditions simulating multi-year field use.

Environmental aging resistance was assessed following the ASTM D7897-18 protocol, which standardizes durability evaluation for materials exposed to soiling and ultraviolet (UV) radiation. This procedure simulates 3 years of natural soiling and 1 year of UV irradiation equivalent to Florida sunshine (see details in Note S9, Supporting Information).[42] During testing, the coated glass was sprayed with a representative soiling mixture (comprising mineral dust, organic debris, and carbon black) suspended in water, followed by exposure to cyclic UV radiation and environmental aging conditions. Optical transmittance and surface wettability were monitored throughout the testing period. As shown in Figure 4d–g, the coated surface maintained a high visible transmittance of ~91.3% and a stable water contact angle of ~167°, with negligible changes in sliding angle, confirming excellent resistance to aging-induced degradation. These performance metrics are comparable or superior to state-of-the-art anti-soiling coatings previously reported in the literature[38] and are critical for preserving photovoltaic efficiency over time (see detailed comparison in Note S10, Supporting Information). In addition to environmental weathering, the thermal stability of the coating was evaluated by subjecting the coated glass to prolonged heat exposure at 100 °C for 1000 h (see Note S9, Supporting Information). During the thermal aging process, the coating consistently preserved its optical transparency and superhydrophobic performance, as evidenced by the data in Figure 4h,i. To further assess the coating's durability, we implemented another rigorous stress-testing protocol, involving continuous solar irradiation at one sun for 1000 h (see Note S9, Supporting Information). Across all tested conditions, the coated glass consistently retained its superhydrophobicity and high optical transparency, demonstrating remarkable resistance to key environmental stressors such as natural dust deposition, prolonged solar

© 2026 The Author(s). *Energy & Environmental Materials* published by John Wiley & Sons Australia, Ltd on behalf of Zhengzhou University.

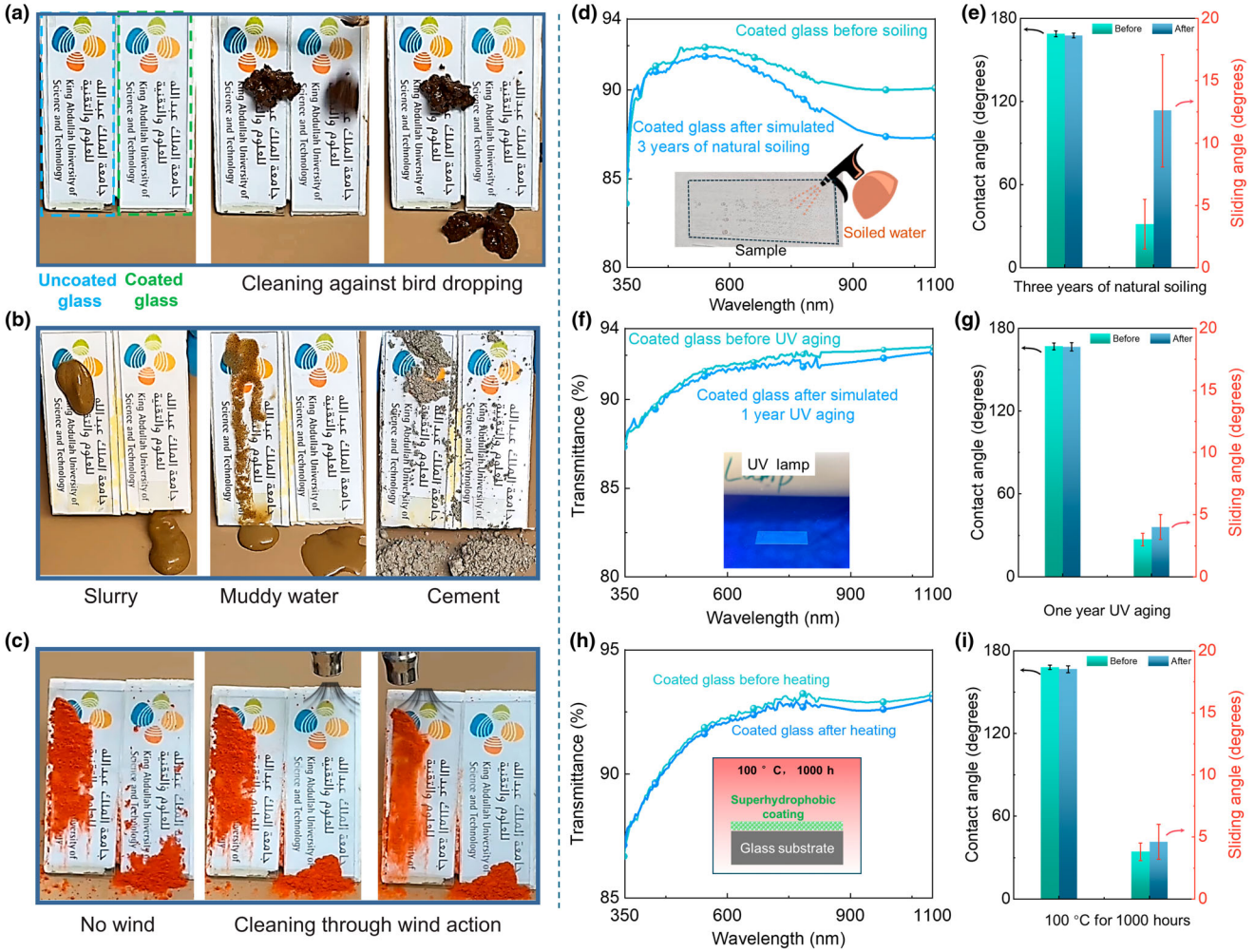


Figure 4. Anti-soiling Performance and Durability Evaluation. a–b) Optical photographs comparing the initial and final states of coated and uncoated glass surfaces subjected to representative environmental soiling agents: a) Bird droppings; b) Slurry, muddy water, and cement particles. The coated surfaces enable easy removal of contaminants without mechanical cleaning, confirming the passive self-cleaning capability. c) Photographs showing wind-assisted dust removal, in which airborne dust is effectively displaced from the coated surface, while remaining adhered to the uncoated glass under identical wind exposure. d, e) Optical transmittance (d) and water contact/sliding angle (e) measurements before and after artificial soiling and weathering, simulating 3 years of natural outdoor exposure according to ASTM D7897-18. f, g) Optical transmittance (f) and wetting behavior (g) before and after one year's equivalent of ultraviolet (UV) aging. h, i) Optical transmittance (h) and water contact/sliding angle (i) measured before and after thermal aging at 100 °C for 1000 h. Across all conditions, the coated glass retains excellent transparency and superhydrophobicity, confirming its long-term robustness under thermal, UV, and environmental stress.

irradiation, high-temperature exposure, and intense ultraviolet radiation.

The long-term durability of the coating is rooted in the intrinsic chemical and morphological stability of its thermally induced silica-based framework. Central to this stability is the formation of a robust Si–O–Si backbone during heat treatment, which exhibits a high bond dissociation energy (~452 kJ mol^{-1}), making it highly resistant to both thermal degradation and UV-induced photolysis (typical photon energies: 375–430 kJ mol^{-1} for 280–320 nm UV).[43] In contrast, terminal hydrophobic groups such as Si–CH_3 contain weaker Si–C (301–318 kJ mol^{-1}) and C–H (412 kJ mol^{-1}) bonds, which are more prone to cleavage under prolonged UV exposure.[43] This makes the surface –CH_3 groups susceptible to photo-oxidative degradation, gradually converting them into hydrophilic silanol (–OH) groups and reducing water repellency. Nevertheless, the underlying nanostructured roughness remains intact, helping to sustain superhydrophobicity over extended exposure.

On the other hand, while partial photodegradation of surface-bound –CH_3 groups may occur, several factors contribute to the sustained superhydrophobicity and optical performance of the coating. First, the underlying nanostructured roughness—established during thermal curing and reinforced by the inclusion of SiO_2 nanoparticles—remains physically intact, preserving the hierarchical surface topology required for air entrapment and low solid–liquid contact. Second, UV-induced degradation is often surface-limited and incomplete, allowing partial retention of hydrophobic functionality even after extended irradiation.

© 2026 The Author(s). *Energy & Environmental Materials* published by John Wiley & Sons Australia, Ltd on behalf of Zhengzhou University.

Third, the densely crosslinked Si–O–Si network offers mechanical and chemical protection to embedded or partially shielded $–CH_3$ groups, delaying full oxidation.[42] Finally, the silica-rich matrix maintains excellent optical transparency, enabling stable solar transmittance through the coating even after aging.[31] Collectively, the abovementioned factors ensure that the coating preserves its key functionalities—including strong water repellency and high visible transmittance—under sustained environmental and thermal stress. This highlights its potential for sustained, low-maintenance operation, facilitating the integration of PV, water harvesting, and agriculture in outdoor agrivoltaics systems.

2.7. Outdoor RC-Induced Condensation for Self-Cleaning Solar Panels and Co-Located Irrigation

To evaluate the real-world applicability of the multifunctional coating, it was applied onto the glass cover of a commercial photovoltaic (PV) panel and tested outdoors at KAUST, Saudi Arabia, from March to September 2024 (**Figure 5a**). The 6-month field experiment aimed to assess both the long-term self-cleaning capability and the water-harvesting potential of the coating under natural environmental conditions. A water-collecting plate was installed beneath each panel to capture condensed water, which was then directed into a storage bottle for quantitative collection and subsequent irrigation demonstration.

2.7.1. Condensation Mechanism and Surface-Dependent Behavior

As demonstrated in Figure 5b,c, condensation was observed on both coated and uncoated glass surfaces during nighttime, coinciding with the surface temperature approaching the dew point under favorable ambient conditions. Continuous measurements of ambient temperature, relative humidity, and dew point (Figure 5d) confirmed that condensation consistently occurred once the surface temperature fell below the dew point (see Note S11 and Videos S8 and S9, Supporting Information).

Distinct condensation behaviors were observed on the coated and uncoated surfaces. On the superhydrophobic coating, small spherical droplets initially nucleated, rapidly coalesced, and subsequently detached and rolled off under gravity (Figure 5b). This condensation process, followed by droplet shedding (yellow arrow), facilitated passive dust removal, enabling autonomous self-cleaning without any external water or energy input. In contrast, on the bare hydrophilic glass, condensed droplets were strongly pinned due to high surface adhesion (zoomed-in view in Figure 5c), gradually merging into larger droplets or continuous liquid films before eventually sliding downward—approximately 6 h later than those on the superhydrophobic surface (Figure 5c). Such delayed and pinned condensation behavior hindered effective particle removal and often resulted in dried residue deposition (see more details in Note S11, Supporting Information).

The superior condensation performance of the superhydrophobic surface compared to untreated glass arises from the combined effects of its thermophysical and structural characteristics. First, the coating possesses slightly higher mid-infrared emissivity within the 8–13 μm atmospheric window, enhancing radiative heat dissipation to the sky and producing a marginally lower surface temperature (black circle in Figure 5d). Even a small temperature drop below ambient significantly increases condensation potential under humid conditions. Second, the hierarchical nanostructure provides abundant heterogeneous nucleation sites, lowering the energy barrier for phase transition and accelerating droplet formation.[41] Moreover, the low contact-angle hysteresis promotes rapid droplet shedding, continually renewing the surface for successive condensation cycles.[42,43] Finally, air pockets trapped within the textured surface may reduce convective heat gain, further amplifying the radiative cooling effect. Significantly, this accelerated droplet shedding also enhances the efficiency of atmospheric water collection, a function which will be discussed later. These synergistic mechanisms collectively enhance condensation efficiency and promote frequent droplet shedding, sustaining the coating's autonomous self-cleaning capability.[44–46]

2.7.2. Long-Term Self-Cleaning and PV Efficiency Retention

As shown in Figure 5e, the coated panel remained visibly cleaner than the uncoated one throughout the test. After 6 months, the uncoated panel showed heavy soiling, while the coated surface retained optical clarity. Electrical performance testing supported these observations: the coated panel maintained efficiency from 18.62 to 18.33% and P_{max} from 4.54 to 4.47 W—a negligible 1.5% drop over 6 months. By contrast, the uncoated panel's efficiency fell from 18.36% to 15.15% and P_{max} from 4.48 to 3.22 W, a 28% loss. Overall, this corresponds to a net power conversion efficiency gain of 3.18% (18.33% vs. 15.15%) for the coated panel at the end of the 6-month field test (Figure 5f). Full-day monitoring (Figure 5g) in the fourth month of the experiment further confirmed the stable performance of the coated panel (18.56% efficiency) versus the continued decline of the uncoated one (14.40%). An efficiency gain of 4.16% was achieved through the coating's self-cleaning action, demonstrating its potential to significantly enhance long-term energy yield and reduce maintenance in real-world PV installations.

2.7.3. Enhanced Dew Collection and Water Quality Validation

Beyond self-cleaning, the coating substantially improved dew collection. Under nighttime relative humidity of 72–92%, a 20 cm × 20 cm coated surface yielded 5.9 g of condensed water, compared with 3.2 g for uncoated glass (Figure 5h). Accounting for the contribution of the collecting plate, the coated surface achieved 128 g $m^{-2}day^{-1}$—a 113% increase over the untreated panel (see detailed estimation in Note S12, Supporting Information). The collected water exhibited low concentrations for most ionic (Na^+, K^+, Mg^{2+}), comparable to commercial drinking water. The higher Ca^{2+} concentration in our collected condensate, compared to the commercial water, is likely attributed to the dissolution of calcium-rich mineral dust from the atmosphere during open-air collection. This natural incorporation of atmospheric dust results in a calcium level that can be beneficial for irrigation purposes.[47] To further assess water quality, heavy metal concentrations (e.g., Pb, As, and Cd) in the collected water were measured, and all values were below WHO guideline limits[48] (see Note S13, Supporting Information, for details). Overall, the harvested water meets WHO standards for both drinking and irrigation purposes[48] (Figure 5i; detailed analysis in Note S13, Supporting Information). Using just 1 g per day, this water supported the successful cultivation of *Brassica rapa chinensis* (Figure 5j), demonstrating practical utility for irrigation.

© 2026 The Author(s). *Energy & Environmental Materials* published by John Wiley & Sons Australia, Ltd on behalf of Zhengzhou University.

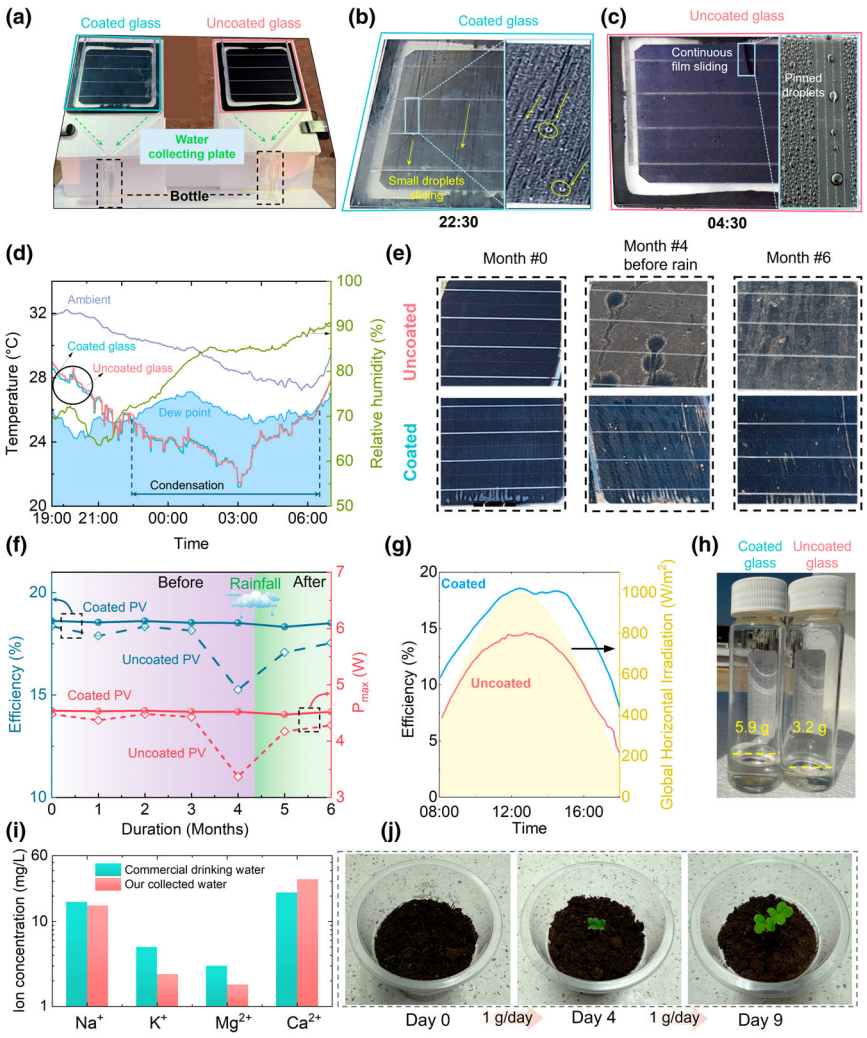


Figure 5. Outdoor performance evaluation of transparent superhydrophobic coating on solar panels under natural environmental exposure. a) Setup for observation of RC-induced condensation and self-cleaning behavior on the coated solar panel at KAUST, Saudi Arabia (June 25, 2025). b) Dew formation on the superhydrophobic coated glass. c) Dew formation on the hydrophilic uncoated glass. d) Corresponding environmental conditions (ambient temperature and relative humidity), along with measured surface temperatures of coated and uncoated glass substrates. Condensation occurs when surface temperature falls below the dew point, confirming RC-induced water formation. e) Optical photographs of uncoated and coated solar panels at Month 0, Month 4 (prior to rainfall), and Month 6, illustrating progressive soiling on the uncoated panel and preserved cleanliness on the coated one. f) Time-resolved measurements of photovoltaic efficiency and maximum output power (P_{max}) over 6 months of outdoor exposure. The green shaded region indicates the partial recovery in uncoated panel performance following a natural rainfall event. g) Efficiency comparison of coated and uncoated solar panels after 4 months of field deployment (August 8, 2024, prior to rainfall), highlighting superior performance retention of the coated system under dusty environmental conditions. h) Comparison of condensed water yield between different surfaces. i) Ionic concentration of the collected freshwater compared with commercial drinking water. j) Demonstration of *Brassica rapa chinensis* cultivation using the collected water.

These results highlight that integrating radiative cooling with PV panels can simultaneously sustain solar panel performance and enable reliable water recovery. Moreover, the presence of vegetation can increase local humidity, further enhancing dew formation and creating a positive feedback loop that strengthens the energy–water–food sustainability nexus in outdoor agrivoltaics systems.

3. Conclusion

This study presents a transparent superhydrophobic coating that addresses long-standing challenges of dust accumulation and environmental aging on photovoltaic (PV) panels and glass surfaces. Fabricated through a simple, solvent-free heat treatment of a food-grade silicone lubricant, the coating provides dual functionality by combining passive radiative cooling with moisture-driven self-cleaning. With high solar transparency (91.3%) and enhanced mid-infrared emissivity (0.90 in the 8–13 μm atmospheric window), the coated surface achieves effective nighttime cooling and dew condensation, which in turn enables natural dust removal without external water or manual cleaning. The coating demonstrates strong repellency against diverse soiling agents —including bird droppings, natural dust, water muddy and cement particles—and retains performance after accelerated aging equivalent to 3 years of outdoor exposure. Field tests in the Saudi Arabia confirmed its durability, with coated panels showing only ∼1.5% relative power loss after 6 months, compared to ∼28% for uncoated panels, corresponding to a net power conversion efficiency gain of 3.18% (18.33% vs. 15.15%). Beyond self-cleaning, the RC–driven condensation also enables efficient dew harvesting, achieving a water yield of 128 g m^{-2} per night—over twice that of untreated panels. The collected water exhibited low ionic concentrations, met WHO standards, and was successfully used to cultivate *Brassica rapa chinensis*, demonstrating practical potential for direct irrigation. This multifunctional, eco-friendly coating therefore not only sustains PV performance with minimal maintenance but also provides a supplementary source of freshwater, paving the way for integrated PV–agriculture systems that jointly deliver clean energy and support plant growth, thereby fostering synergistic energy–water–food sustainability.

4. Experimental Section

Contact angle and surface profilometry: The water contact angle (WCA) and sliding angle (SA) were measured using a computer-controlled goniometer system (Contact angle measurement, Kruss). For WCA measurements, a 5 μL water droplet was dispensed onto the surface, and the average value was obtained from at least three measurements, with error bars shown in the respective figures. The SA was measured using the tilting method. The surface roughness of the samples was measured with an optical profilometer (New View 7300-Zygo Optical Profiler) using the coherence scanning interferometry method. The surface average roughness values were analyzed with the optical profilometer using a 20 × objective lens.

© 2026 The Author(s). *Energy & Environmental Materials* published by John Wiley & Sons Australia, Ltd on behalf of Zhengzhou University.

Spectral performance measurement: For visible spectrum, reflection measurements were carried out using a spectrometer (Perkin Elmer Lambda 950) equipped with tungsten-halogen and deuterium lamps. Forward and backward scattered light was captured with a 150 mm visible/near-infrared integrating sphere coupled with a photomultiplier detector. For measurements in the mid-infrared portion of the spectrum, a Fourier transform infrared spectrometer (Bruker HYPERION II), an integrating sphere (A562-G/Q) coated with diffuse gold reflectors, and a DLaTGS detector were used.

Acknowledgements

S.D., A.R.S. and M.G. contributed equally to this work. This work was partially supported by KAUST (BAS/1/1415-01-01), KAUST COE: CREST (FCC/1/5937-06), and CRG12 (URF/1/6395-01). The authors thank Afrah Harafan and Ahmed Saleque for their assistance with the ion-concentration characterization of the collected water.

Conflict of Interest

A patent disclosure has been submitted through KAUST.

Supporting Information

Supporting Information is available from the Wiley Online Library or from the author.

Keywords

agrivoltaics, radiative cooling, self-cleaning, superhydrophobic, water harvesting

Received: December 8, 2025
Revised: February 9, 2026
Published online: February 23, 2026

[1] International Energy Agency (IEA), *World Energy Outlook 2018*, IEA, Paris **2018**.
[2] U.S. Energy Information Administration (EIA), *International Energy Outlook 2019*, EIA, Washington, DC **2019**.
[3] G. A. Barron-Gafford, M. A. Pavao-Zuckerman, R. L. Minor, L. F. Sutter, I. Barnett-Moreno, D. T. Blackett, M. Thompson, K. Dimond, A. K. Gerlak, G. P. Nabhan, J. E. Macknick, *Nat. Sustainability* **2019**, *2*, 848.
[4] S. Ghasemi, I. Sadeghkhani, *Sol. RRL* **2025**, *9*, 202500041.
[5] K. Ilse, L. Micheli, B. W. Figgis, K. Lange, D. Daßler, H. Hanifi, F. Wolfertstetter, V. Naumann, C. Hagendorf, R. Gottschalg, J. Bagdahn, *Joule* **2019**, *3*, 2303.
[6] H. Niu, S. Luo, X. Yao, T. Li, M. Ai, R. Zhou, H. Wang, L. Wan, Y. Du, L. Hu, B. Xu, J. Xu, *Mater. Sci. Semicond. Process.* **2023**, *166*, 107741.
[7] S. Panat, K. K. Varanasi, *Sci. Adv.* **2022**, *8*, eabn9204.
[8] B. L. S. Nomeir, S. Bouchareb, M. Aillerie, S. Naamane, *Sol. Energy Mater. Sol. Cells* **2023**, *257*, 112347.
[9] D. Dahlioui, B. Laarabi, A. Barhdadi, *Sustain. Energy Technol. Assess.* **2022**, *49*, 101774.
[10] H. Fang, S. Dang, P. Kumar, J. Wang, L. Xu, Y. Zhu, A. Almogbel, A. Albadri, S. de Wolf, Q. Gan, *Mater. Sci. Eng. R. Rep.* **2025**, *165*, 101016.
[11] H. Fang, L. Zhou, L. Xu, S. Dang, S. De Wolf, Q. Gan, *iScience* **2024**, *27*, 108806.
[12] S. M. F. Zhang, J. P. Seif, M. D. Abbott, A. H. T. Le, T. G. Allen, I. Perez-Wurfl, Z. Hameiri, *Nano Energy* **2022**, *98*, 107221.
[13] S. Saboor, P. Vigneshwaran, R. Abin, K. Karolos, M. Domenico, C. Erdem, S. C. Ahamed, A. Mamdooh, K. Sher, G. Ali, A. Ümit, *Case Stud. Therm. Eng.* **2023**, *48*, 103128.
[14] K. A. M. Ali, Y. K. O. T. Osman, G. G. A. El-Wahhab, T. A. M. Abdelwahab, A. E. M. Fodah, *Sci. Rep.* **2025**, *15*, 8211.
[15] S. Sutha, S. Suresh, K. R. Ravi, *Sol. Energy Mater. Sol. Cells* **2017**, *165*, 128.
[16] S. A. Tayel, A. E. Abu El-Maaty, E. M. Mostafa, Y. F. Elsaadawi, *Sci. Rep.* **2022**, *12*, 21236.
[17] Z. Zhang, L. Dong, M. Dong, S. Ruan, Z. Chen, *Sci. China Technol. Sci.* **2026**, *69*, 1120104.
[18] W. Li, M. Dong, L. Fan, J. J. John, Z. Chen, S. Fan, *ACS Photonics* **2021**, *8*, 269.
[19] K. Yang, X. Wu, L. Zhou, P. Wu, I. Gereige, Q. Gan, *Nat. Rev. Clean Technol.* **2025**, *1*, 235.
[20] H. Cho, D. Preston, Y. Zhu, E. N. Wang, *Nat. Rev. Mater.* **2017**, *2*, 16092.
[21] T. Mouterde, G. Lehoucq, S. Xavier, A. Checco, C. T. Black, A. Rahman, T. Midavaine, C. Clanet, D. Quéré, *Nat. Mater.* **2017**, *16*, 658.
[22] S. Dang, H. H. Almahfoudh, A. M. Alajlan, H. Qasem, J. Wang, Y. Zhu, O. M. Bakr, B. S. Ooi, Q. Gan, *Light Sci. Appl.* **2025**, *14*, 100.
[23] K. C. Park, H. J. Choi, C. H. Chang, R. E. Cohen, G. H. McKinley, G. Barbastathis, *ACS Nano* **2012**, *6*, 3789.
[24] M. Zhou, H. Song, X. Xu, A. Shahsafi, Y. Qu, Z. Xia, Z. Ma, M. A. Kats, J. Zhu, B. S. Ooi, Q. Gan, Z. Yu, *Proc. Natl Acad. Sci. USA* **2021**, *118*, e2019292118.
[25] W. Li, Y. Shi, K. Chen, L. Zhu, S. Fan, *Acs Photonics* **2017**, *4*, 774.
[26] L. Zhu, A. Raman, K. X. Wang, M. A. Anoma, S. Fan, *Optica* **2014**, *1*, 32.
[27] A. Rahman, A. Ashraf, H. Xin, X. Tong, P. Sutter, M. D. Eisaman, C. T. Black, *Nat. Commun.* **2015**, *6*, 5963.
[28] S. Ji, K. Song, T. B. Nguyen, N. Kim, H. Lim, *ACS Appl. Mater. Interfaces* **2013**, *5*, 10731.
[29] C. Guo, H. Tang, P. Wang, Q. Xu, H. Pan, X. Zhao, F. Fan, T. Li, D. Zhao, *Nat. Commun.* **2024**, *15*, 6100.
[30] L. Zhu, A. P. Raman, S. Fan, *Proc. Natl Acad. Sci. USA* **2015**, *112*, 12282.
[31] A. R. M. Siddiqui, K. Balani, *J. Mater. Chem. A* **2017**, *5*, 2936.
[32] Y. Wu, J. Du, G. Liu, D. Ma, F. Jia, J. J. Klemeš, J. Wang, *Renew. Energy* **2022**, *185*, 1034.
[33] S. Li, K. Page, S. Sathasivam, F. Heale, G. He, Y. Lu, Y. Lai, G. Chen, C. J. Carmalt, I. P. Parkin, *J. Mater. Chem. A* **2018**, *6*, 17633.
[34] S. Ahmad, A. R. Siddiqui, K. Yang, M. Zhou, H. M. Ali, R. Hardian, G. Szekely, D. Daniel, S. Yang, Q. Gan, *Adv. Mater.* **2024**, *36*, 2404037.
[35] T. Aytug, A. R. Lupini, G. E. Jellison, P. C. Joshi, I. H. Ivanov, T. Liu, P. Wang, R. Menon, R. M. Trejo, E. Lara-Curzio, S. R. Hunter, J. T. Simpson, M. P. Paranthaman, D. K. Christen, *J. Mater. Chem. C* **2015**, *3*, 5440.
[36] K. Seo, M. Kim, S. Seok, D. H. Kim, *Colloids Surf. A Physicochem. Eng. Asp.* **2016**, *492*, 110.
[37] A. Syafiq, A. Pandey, N. Adzman, N. Abd Rahim, *Sol. Energy* **2018**, *162*, 597.
[38] F. J. P. Dickhardt, S. Singh, K. K. Varanasi, *Small* **2025**, *21*, 2406723.
[39] Y. Zhou, C. Wang, X. Zeng, Q. Wang, J. Li, L. Zhang, *Appl. Surf. Sci.* **2006**, *253*, 2690.
[40] L. Zhou, X. Yin, Q. Gan, *Nat. Sustainability* **2023**, *6*, 1030.
[41] D. Goswami, S. Manna, G. De, *ACS Appl. Mater. Interfaces* **2011**, *3*, 3440.
[42] J. Song, W. Zhang, Z. Sun, M. Pan, F. Tian, X. Li, M. Ye, X. Deng, *Nat. Commun.* **2022**, *13*, 4805.
[43] L. Delzeit, C. Hunter, presented at 48th International Conference on Environmental Systems **2018**.
[44] C. Liu, J. Fan, H. Bao, *Sol. Energy Mater. Solar Cells* **2020**, *216*, 110676.
[45] H. Budunoglu, A. Yildirim, G. M. Akin, M. Bayindir, *ACS Appl. Mater. Interfaces* **2011**, *3*, 539.
[46] Z. Shen, H. Huang, L. Chen, S. Shi, Z. Guan, *J. Appl. Polym. Sci.* **2014**, *131*, 40387.
[47] E. Epstein, A. J. Bloom, *Mineral Nutrition of Plants: Principles and Perspectives*, 2nd ed., Sinauer Associates, Sunderland, MA **2004**.
[48] World Health Organization, *Guidelines for Drinking-water Quality: Fourth Edition Incorporating the First Addendum*, World Health Organization, Geneva **2017**.

© 2026 The Author(s). *Energy & Environmental Materials* published by John Wiley & Sons Australia, Ltd on behalf of Zhengzhou University.